Elucidating Gating Effects for Hydrogen Sorption in MFU-4-Type Triazolate-Based Metal–Organic Frameworks Featuring Different Pore Sizes

Dmytro Denysenko,[a] Maciej Grzywa,[a] Markus Tonigold,[b] Barbara Streppel,[c] Ivana Krkljus,[c] Michael Hirscher,[c] Enrico Mugnaioli,[d] Ute Kolb,[d] Jan Hanss,[a] and Dirk Volkmer*[a, b]

Abstract: A highly porous member of isoreticular MFU-4-type frameworks, [Zn$_5$Cl$_4$(BTDD)$_3$] (MFU-4*l*(arge)) (H$_2$-BTDD = bis(1*H*-1,2,3-triazolo[4,5-*b*],-[4′,5′-*i*])dibenzo[1,4]dioxin), has been synthesized using ZnCl$_2$ and H$_2$-BTDD in *N*,*N*-dimethylformamide as a solvent. MFU-4*l* represents the first example of MFU-4-type frameworks featuring large pore apertures of 9.1 Å. Here, MFU-4*l* serves as a reference compound to evaluate the origin of unique and specific gas-sorption properties of MFU-4, reported previously. The latter framework features narrow-sized pores of 2.5 Å that allow passage of sufficiently small molecules only (such as hydrogen or water), whereas molecules with larger kinetic diameters (e.g., argon or nitrogen) are excluded from uptake. The crystal structure of MFU-4*l* has been solved ab initio by direct methods from 3D electron-diffraction data acquired from a single nanosized crystal through automated electron diffraction tomography (ADT) in combination with electron-beam precession. Independently, it has been solved using powder X-ray diffraction. Thermogravimetric analysis (TGA) and variable-temperature X-ray powder diffraction (XRPD) experiments carried out on MFU-4*l* indicate that it is stable up to 500 °C (N$_2$ atmosphere) and up to 350 °C in air. The framework adsorbs 4 wt % hydrogen at 20 bar and 77 K, which is twice the amount compared to MFU-4. The isosteric heat of adsorption starts for low surface coverage at 5 kJ mol^{-1} and decreases to 3.5 kJ mol^{-1} at higher H$_2$ uptake. In contrast, MFU-4 possesses a nearly constant isosteric heat of adsorption of ca. 7 kJ mol^{-1} over a wide range of surface coverage. Moreover, MFU-4 exhibits a H$_2$ desorption maximum at 71 K, which is the highest temperature ever measured for hydrogen physisorbed on metal–organic frameworks (MOFs).

Keywords: adsorption · hydrogen · metal–organic frameworks · thermal desorption spectroscopy · triazolates

[a] D. Denysenko, Dr. M. Grzywa, Dr. J. Hanss, Prof. Dr. D. Volkmer
Institute of Physics
Chair of Solid State and Material Science
Augsburg University
Universitätsstrasse 1, 86135 Augsburg (Germany)
Fax: (+49) 821-598-5955
E-mail: dirk.volkmer@physik.uni-augsburg.de

[b] M. Tonigold, Prof. Dr. D. Volkmer
Institute of Inorganic Chemistry II—Materials and Catalysis
Ulm University
Albert-Einstein-Allee 11, 89081 Ulm (Germany)

[c] B. Streppel, I. Krkljus, Dr. M. Hirscher
Max Planck Institute for Metals Research
Heisenbergstrasse 3, 70569 Stuttgart (Germany)

[d] Dr. E. Mugnaioli, Dr. U. Kolb
Institute of Physical Chemistry
Johannes Gutenberg-University Mainz
Welderweg 11, 55099 Mainz (Germany)

Introduction

Hydrogen is an attractive energy carrier that could replace petroleum in the future. However, hydrogen storage is a difficult problem that still has to be solved. Investigation of metal–organic frameworks (MOFs) as porous materials for hydrogen storage is currently an important research field.[1] Due to a recent requirement of the United States Department of Energy, a hydrogen storage tank must contain 6 wt % of hydrogen. Hydrogen uptake depends on several properties of porous material. At low pressure, hydrogen uptake correlates with the heat of adsorption. At intermediate pressure (30 bar), uptake correlates with the surface area, and at high pressure (100 bar and more), uptake correlates with the free volume.[2] Uptake values up to 10 wt % H$_2$ at 100 bar and 77 K were reported for MOF-5.[3] However, a material with a high surface area or free volume alone is not necessarily a good candidate for hydrogen storage.

Relatively high adsorption enthalpy is required for successful application. Calculations[4] show that the adsorption enthalpy of 15 kJ mol^{-1} would be optimal for a reversible adsorption–desorption cycle at room temperature. However, due to very weak van der Waals interactions of H_2 molecules, the heat of hydrogen physisorption typically ranges from 4 to 7 kJ mol^{-1}. Metal–organic frameworks with unsaturated metal sites can reach an adsorption enthalpy of over 10 kJ mol^{-1}.[5] The pore-size distribution of a MOF strongly influences the heat of adsorption. Thus, frameworks with smaller pore sizes have higher heat of adsorption due to a stronger interaction between adsorbed hydrogen molecules and cavities.[6] The desorption temperature of hydrogen likewise increases with decreasing pore size.[7] Monte Carlo calculations have been used to show that pores with a diameter of 7 Å should be optimal for hydrogen adsorption.[8] However, these calculations did not consider the important gating effects of very small apertures or narrow channels interconnecting the internal voids of the storage material. Finally, the stability of a metal–organic framework plays a very important role for its potential use as a hydrogen-storage material as well as for other applications. Thus, the performance of MOF-5 in hydrogen adsorption depends strongly on the preparation and handling conditions since this framework is not stable under ambient conditions owing to its sensitivity towards hydrolytic decomposition.[3]

In a general sense, the success of inventing functional MOFs will rely on a systematic development of suitable secondary building units (SBUs) from which a structurally and functionally diverse class of novel materials might evolve.[9a,b] Herein we present a unique "solid-state construction kit" that is based on novel pentanuclear SBUs, for which the term "Kuratowski-type" SBUs is proposed. We have recently developed two major lines of functional MOF compounds, termed MFU-1 and MFU-4, respectively. MFU-1 is a pyrazolate-based redox-active analogue of the famous MOF-5[9c] featuring four tetrahedrally coordinated Co^{II} centers that are connected by a central μ_4-bridging oxide anion (Figure 1, left). This compound shows enhanced stability against hydrolytic and oxidative decomposition and it can be employed as catalyst in a range of radical-centered oxidation reactions.[10] Since the particular SBU of MFU-1 seems to be limited to the presence of a {Co$_4$O} core, we have developed a modular MOF family (MFU-4),[11] which is based
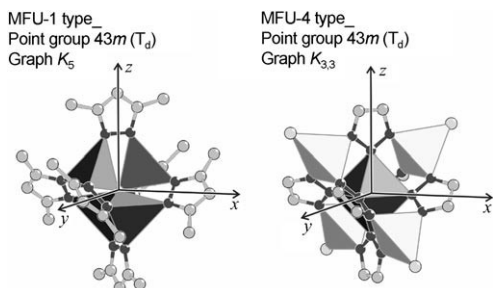
on Kuratowski-type pentanuclear SBUs of the general formula [M^{II}Zn$_4$X$_4$(**L**$_6$)] (Figure 1, right). These feature a central metal ion coordinated to six triazolate ligands (**L**) that span a Cartesian system and can either be assembled into discrete coordination compounds[12] or into porous cubic frameworks.[11] The central metal ion in the octahedral coordination environment can be varied[12] giving the opportunity of potentially obtaining redox-active SBUs that are also Lewis acidic, with chemical properties that can be fine-tuned by selecting appropriate metal ions. Changing the Zn^{2+} ions in tetrahedral positions to other transition-metal ions could improve hydrogen-sorption properties.[5]

The graph theoretical analysis proves that [M^{II}Zn$_4$X$_4$(**L**$_6$)] units contain the nonplanar $K_{3,3}$ graph. According to a theorem of C. Kuratowski,[13] a finite graph is planar only if it does not contain a subgraph that is a subdivision of K_5 (the complete graph on five vertices) or $K_{3,3}$ (a complete bipartite graph on six vertices, three of which connect to each of the other three). As can be seen in Figure 2, the molecular
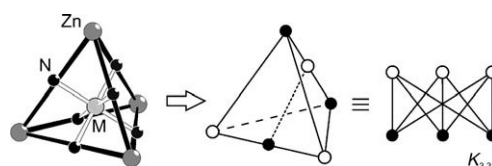

Figure 2. Formal derivation of the $K_{3,3}$ graph, which can be used to represent the connectivity scheme in Kuratowski-type SBUs.

graph of [M^{II}Zn$_4$X$_4$(**L**$_6$)] units in fact contains a subgraph of $K_{3,3}$. Accordingly, there is no way to draw [M^{II}Zn$_4$X$_4$(**L**$_6$)] as a planar graph and thus we propose a pseudoperspective skeletal formula as derived in Figure 3 to represent Kuratowski-type coordination compounds in this paper and in the future.
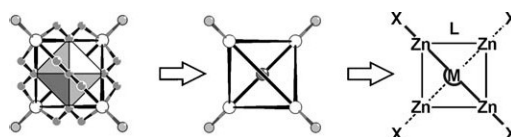

Figure 3. Derivation of a skeletal formula representing the connectivity of [M^{II}Zn$_4$X$_4$(**L**$_6$)] units (X: terminal ligand; **L**: 1,2,3-triazolate-type ligand).

The first triazolate-based MOF featuring Kuratowsky-type secondary building units, MFU-4, was constructed from benzobistriazolate linkers and {Zn$_5$Cl$_4$}$^{6+}$ cores featuring a very high thermal and hydrolytic stability. Due to its small pore apertures (2.5 Å) it is highly selective for the adsorption of atoms or small molecules such as H_2 and it can therefore be applied in molecular sieving applications, some of which are hard to achieve with other kinds of porous materials. However, to separate mixtures of larger molecular adsorbates or for catalytic transformations a porous frame-

Figure 1. Structural features of SBUs found in MFU-1 and MFU-4.

work featuring large pore apertures is required. Herein we describe MFU-4*l*(arge) constructed from bis(1*H*-1,2,3-triazolo[4,5-*b*],[4′,5′-*i*])dibenzo[1,4]dioxin linkers (H₂-BTDD, **2**), which is a novel member of isoreticular MFU-4-type frameworks (Scheme 1).

H₂-BBTA (**1**)   H₂-BTDD (**2**)
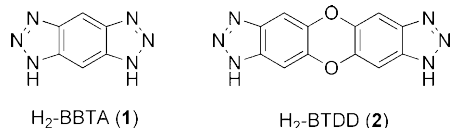
Scheme 1. Triazolate linker **1** for MFU-4 and **2** for MFU-4*l*.

Comparing hydrogen-sorption properties of MFU-4 and MFU-4*l* featuring small and large pores, respectively, might help to improve present concepts about the influence of pore size on the potential of a porous material for hydrogen storage by means of physisorption. In the following we will demonstrate that small pore apertures are responsible for selective hydrogen adsorption in MFU-4. Its small pore diameters result in a higher heat of adsorption due to a stronger interaction between adsorbed molecules and the MOF. This desirable property of MFU-4, however, is compromised by a reduced void volume if compared with MFU-4*l*, which features larger pores and a higher surface area, which allow for uptake of a larger total amount of hydrogen at high pressure. Only a few studies with accurate determination of the isosteric heat of adsorption from isotherms have been reported so far.[6] A powerful tool that can help us to understand the mechanism of adsorption and diffusion of hydrogen in MOFs is thermal desorption spectroscopy (TDS).[7] Herein we present hydrogen-adsorption isotherms for MFU-4 and MFU-4*l* measured over a wide temperature range (77–298 K) as well as TDS studies at low temperatures between 20 and 120 K.

Results and Discussion

Synthesis and characterization: The bis(1*H*-1,2,3-triazolo-[4,5-*b*],[4′,5′-*i*])dibenzo[1,4]dioxin (H₂-BTDD, **2**) ligand was synthesized in three steps starting from dibenzo[1,4]dioxin (see Scheme 2). The nitration of dibenzo[1,4]dioxin described in the literature[14] gives a very low yield (17%) of the desired product and requires several purification steps. Therefore, we have developed an improved and simple procedure that allowed us to obtain 2,3,7,8-tetranitrodibenzo-[1,4]dioxin (**3**) in good yield. The reduction of the nitro compound was carried out according to the literature procedure.[15]

MFU-4*l* can be synthesized in high yield using solvothermal or microwave methods and *N*,*N*-dimethylformamide (DMF) as a solvent (see Scheme 3).

Different ratios of ZnCl₂/**2** (from 2:1 to 40:1) can be used for MOF synthesis. However, a large excess amount of zinc chloride is preferable to avoid the formation of amorphous
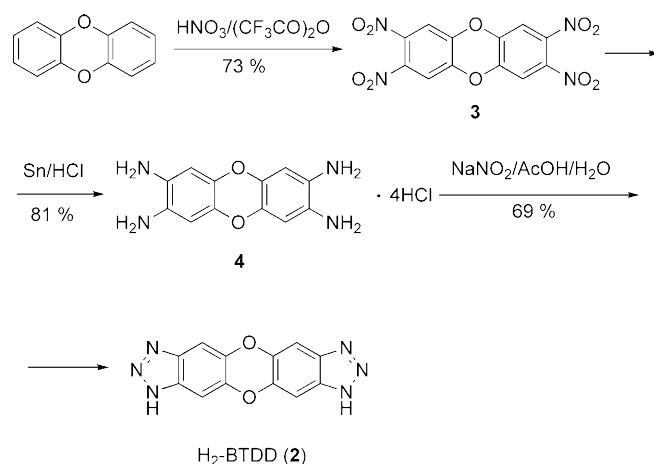
Scheme 2. Synthesis of ligand **2**.
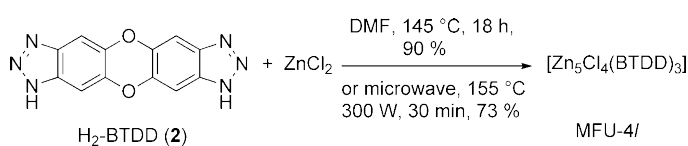
Scheme 3. Synthesis of MFU-4*l*.

byproducts that have been observed when using low metal/ligand ratios. The ratio of 20:1 was found to be optimal. MFU-4*l* was obtained as a microcrystalline powder with typical crystal sizes ranging from 1 to 5 μm (Figure 4). Crystals of this size are not suitable for single-crystal X-ray structure analysis, thus powder X-ray diffraction and single-crystal electron diffraction have been used for structural characterization.
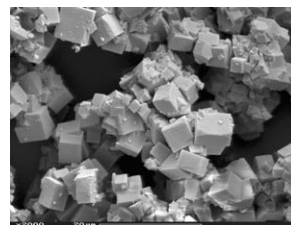

Figure 4. SEM image of MFU-4*l* prepared by the solvothermal method (scale bar: 20 μm).

The use of *N*-methylpyrrolidone (NMP) as solvent offers the advantage of a higher solubility of the linker. Also, some larger crystals, up to 40 μm, could be obtained in NMP under solvothermal conditions. However, the yield was very poor and the product contains a considerable amount of amorphous impurities.

Structure solution by electron diffraction: Automated electron diffraction tomography (ADT)[16–18] is a new technique in which the reciprocal space is sampled by tilting a nano-sized single crystal in small steps over the full tilt range ac-

cessible in the transmission electron microscope. We used nanobeam electron diffraction to create a low-dose, small, semiparallel electron beam and scanning TEM to image and track the crystal; this technique is particularly suitable for beam-sensitive materials that are normally not accessible by conventional electron-diffraction techniques.[19] After reconstruction of the 3D reciprocal space, cell parameter determination with a maximum error of 5% is possible. The intensities that can be observed after indexing are already quasi-kinematical and cover most of the symmetrically independent reciprocal space. ADT can be combined with precession electron diffraction (PED), thus integrating the space between the tilts to enhance intensity quality further. Based on ADT data sets, the full structure can be found ab initio by direct methods in a pure kinematical approach. This technique was able to solve complex nanoporous structures such as charoite.[20] A cubic face-centered cell ($a = 32.0(4)$ Å) was automatically determined. No further extinction was detected in the reconstructed three-dimensional reciprocal space (Figure 5). All independent reflections up to a resolution of
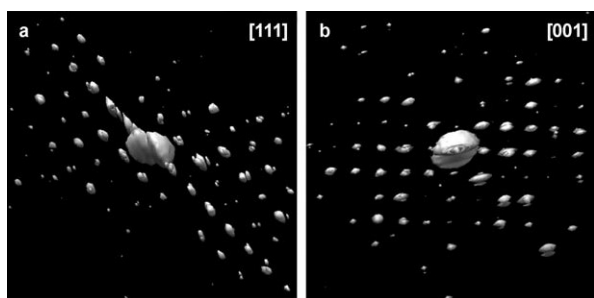

Figure 5. Projections of three-dimensional reconstructed reciprocal space by ADT data: a) [111] projection; b) [001] projection.

1.3 Å were sampled and integrated. Intensities collected in such a way were quasi-kinematical because they were integrated from nonoriented diffraction patterns. The amount and quality of the data obtained by ADT is remarkably superior to any previous electron-diffraction experiment performed on MOFs, for which cell parameters were determined by single-oriented projections.[21] Ab initio structure solution delivered the complete structure directly except for one carbon atom. The structure was refined by imposing a rigid benzene ring and soft bond restraints. The final residual R value was 32.1%, which is in an acceptable range for electron-diffraction data.

Crystal structure description: The crystal structure of MFU-4*l* has been independently solved ab initio from powder X-ray diffraction data by direct methods. Both structure solutions—from powder X-ray and ADT diffraction data, respectively—deliver almost identical structures, which show small differences in bond lengths only. The maximum deviation in atom positions from the ADT solution is 0.2 Å. The crystal structure of MFU-4*l* is similar to that of MFU-4 (Figure 6) in that it possesses a cubic six-connected net. This
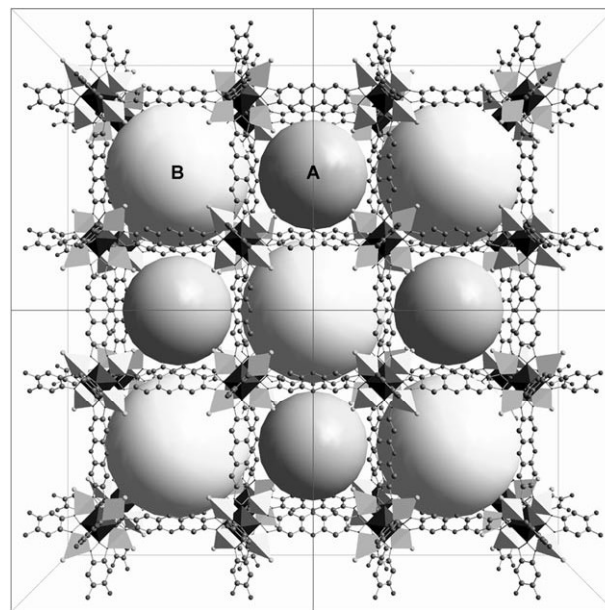

Figure 6. Ball-and-stick representation of the MFU-4*l* framework along the crystallographic *a* direction (octahedrally coordinated Zn²⁺: dark-gray octahedra; tetrahedrally coordinated Zn²⁺: pale-gray tetrahedra). All hydrogen atoms are omitted for clarity. The larger spheres represent the cavities of **B** cells, whereas the smaller spheres represent the cavities of **A** cells.

can be described as follows: the nodes (vertices) are represented by cationic pentanuclear $\{Zn_5Cl_4\}^{6+}$ clusters and the links (edges) of the net are represented by finite rods of $BTDD^{2-}$ anions. There are two types of Zn ions: first, a tetrahedrally coordinated zinc atom (Zn1) with $3m$ site symmetry is surrounded by three N atoms from BTDD ligands (forming the base of the tetrahedron) and one Cl atom (constituting the apex of the tetrahedron); second, an octahedrally coordinated zinc atom (Zn2), with $\bar{4}3m$ site symmetry surrounded by six N atoms from six hexadentate-coordinated BTDD ligands. All BTDD ligands are twisted around their coordinative bonds to the central Zn2 ions. In the solution from the powder X-ray diffraction data, the distances Zn–N for a tetrahedrally coordinated Zn atom are smaller (2.010(5) Å) than those between octahedrally coordinated Zn atoms and nitrogen donors (2.0414(9) Å). In the ADT solution, the distances Zn–N for a tetrahedrally coordinated Zn atom are 2.09(3) Å and for a octahedrally coordinated Zn atom are 2.12(4) Å, respectively. These values are in good agreement with other Zn–triazolate complexes (1.98–2.05 Å for tetrahedral coordination and 2.14–2.22 Å for octahedral coordination).[11]

According to the results obtained by using the PLATON/SQUEEZE[22] program, the total potentially accessible void volume is 23563.2 Å³, which is 78.7% of the unit-cell volume.

Analogously to MFU-4, the framework of MFU-4*l* has two different types of cavities (the smaller and the larger ones are referred to as **A** and **B** cells, respectively) arranged in an alternating fashion (Figure 6). The **A** cells are repre-

sented by the cubic arrangement of eight chlorine atoms that have a minimum nonbonding distance of 8.9320(2) Å from each other. Taking the van der Waals radii of Cl atoms (1.75 Å) into account, imaginary spheres with a diameter of 11.97 Å could fit into the **A** cells. Each of the larger **B** cells, on the other hand, is surrounded by twelve dioxin rings and an imaginary sphere with a diameter of 18.56 Å would fit into it, taking the van der Waals radii of the C atoms into account. The aperture between **A** and **B** cells would admit the passage of an imaginary sphere with a diameter of 9.13 Å (taking the van der Waals radii of Cl atoms into account.

Large pore apertures in MFU-4l allow the adsorption and free diffusion of larger molecules. Table 1 shows selected structural parameters of MFU-4 and MFU-4l for comparison.

Table 1. Selected structural features of MFU-4 and MFU-4l.

	MFU-4	MFU-4l
space group	$Fm\bar{3}m$ (225)	$Fm\bar{3}m$ (225)
cell length $a=b=c$ [Å]	21.6265(9)	31.057(1)
V [Å^3]	10114(9)	29955(4)
ρ_{calcd} [g cm^{-3}]	1.23	0.56
void volume [%]	53.1	78.7
diameter **A** cells [Å]	3.88	11.97
diameter **B** cells [Å]	11.94	18.56
aperture [Å]	2.52	9.13

Thermal analyses: Due to a larger pore size, MFU-4l loses solvent molecules much easier then MFU-4. Thus, MFU-4l heated in a vacuum at 180°C contains no solvent as observed by thermogravimetric analysis (TGA) and shows no weight loss up to 500°C (Figure 7). In contrast, MFU-4 must be heated at 250°C under vacuum to remove DMF molecules, which cannot pass through small apertures easily.
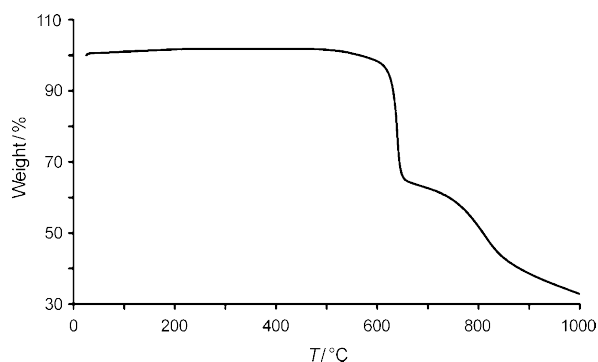

Figure 7. Temperature-dependent weight-loss of MFU-4l (sample exposed to flowing nitrogen gas).

By using more accurate TGA/MS measurements on the sample stored in air, traces of adsorbed molecules were detected (Figure 8). Weight loss below 200°C corresponds to water (m/z 18). The second peak with m/z 44 observed in
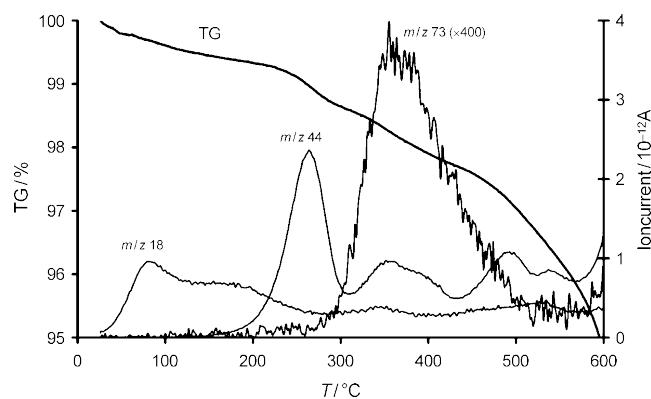

Figure 8. TGA/MS data of MFU-4l.

the temperature range between 200 and 300°C corresponds to CO$_2$, which was also identified by TGA/IR spectroscopy. The third peak is DMF (m/z 73 for the molecular ion and m/z 44 for (CH$_3$)$_2$N$^+$).

The presence of DMF was further confirmed by using a thermodesorption GC-MS trace of volatile products formed after heating MFU-4l at 260°C.

Variable-temperature X-ray powder diffraction (VTXRPD) studies (Figure 9a) showed that MFU-4l is stable up to 350°C in air, which is similar to the stability of MFU-4. Small differences in the intensities of the reflections are observed at higher temperatures due to the removal of residual solvent molecules. At 400°C, zinc oxide (PDF no. 36-1451) appears as a new crystal phase that predominates
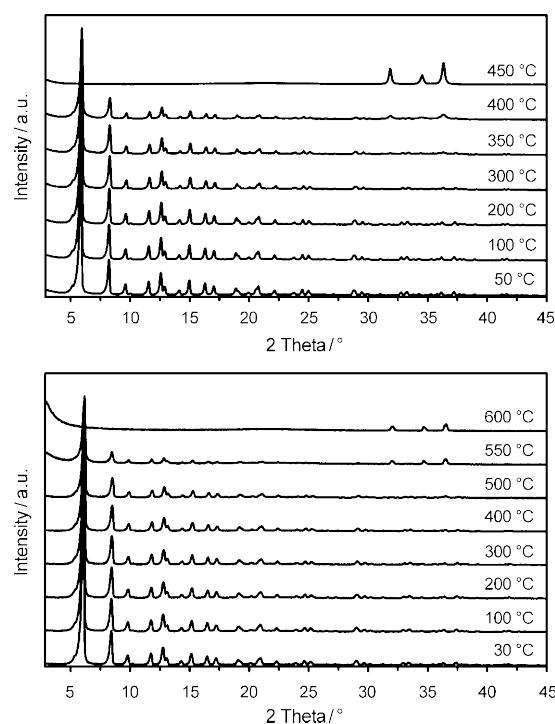

Figure 9. VTXRPD plots of MFU-4l in the range of a) 50–450°C under air and b) 30–600°C under a nitrogen atmosphere.

above 450 °C, at which the framework is completely decomposed. Under a nitrogen atmosphere it is stable even up to 500 °C (Figure 9b), which is in agreement with TGA measurements.

Physisorption results: MFU-4*l* exhibits permanent porosity, which was confirmed by argon gas sorption. Prior to measurement, the sample was suspended multiple times in dichloromethane, which led to solvent exchange of less-volatile DMF molecules. The sorption isotherm of MFU-4*l* obtained with Ar gas reveals a type-I sorption behavior, which is characteristic of microporous solids (Figure 10). The pore
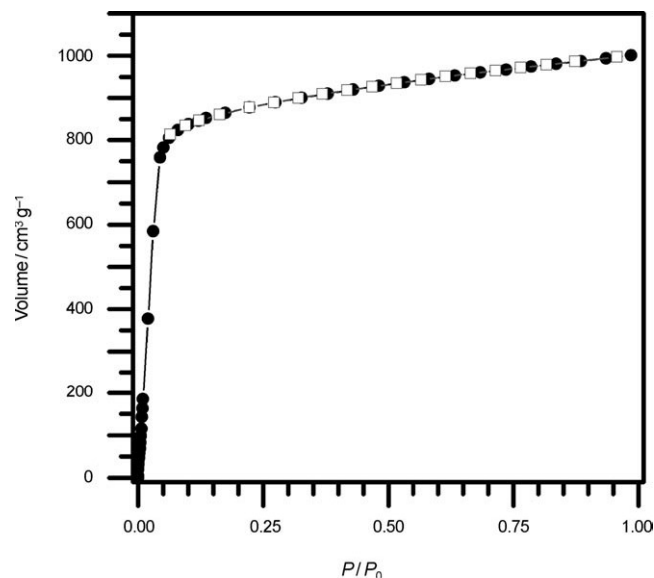

Figure 10. Representative argon adsorption isotherm at 77 K for a desolvated sample of MFU-4*l* (●: adsorption, □: desorption).

volume obtained from the sorption isotherm at $P/P_0 = 0.9$ is $1.26 \text{ cm}^3\text{g}^{-1}$ ($1.15 \text{ cm}^3\text{g}^{-1}$ pore volume and 1.93 nm pore diameter determined by the Dubinin–Radushkevich equation),[23] which is close to the value expected from the crystallographic data ($1.42 \text{ cm}^3\text{g}^{-1}$ for the solvent-free crystal and 1.86 nm pore diameter). The adsorption data was fitted to the BET equation to give a surface area of $2750 \text{ m}^2\text{g}^{-1}$ for MFU-4*l*,[24] which is close to the theoretical values of the specific surface area of $2987 \text{ m}^2\text{g}^{-1}$ as derived from the crystal structure by a Monte Carlo integration technique (in which a probe molecule, here argon, is "rolled" over the surface).[24] Experimental values of MFU-4 and MFU-4*l* are compared in Table 2.

Table 2. Measured and calculated[24] specific surface areas.

Framework	Adsorbate	Specific surface area [m² g⁻¹]	
		Calculated	Measured
MFU-4	H_2	1736	
MFU-4	Ar	1350	ca. 0
MFU-4*l*	H_2	3095	
MFU-4*l*	Ar	2987	2750

To evaluate the pore-size distribution of MFU-4*l*, the argon-sorption isotherms sampled at 77 K were analyzed using nonlocal density functional theory (NLDFT)[25] implementing a carbon equilibrium transition kernel for argon adsorption at 77 K based on a slit-pore model.[26] The distributions calculated by fitting the adsorption data (Figure 11)
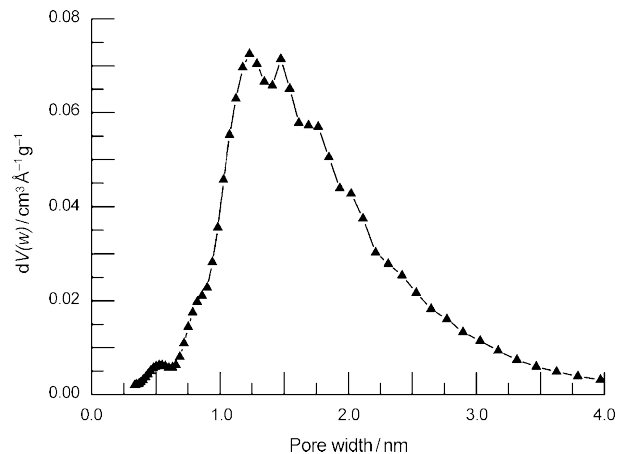

Figure 11. Pore-size distribution for MFU-4*l* calculated by fitting NLDFT models to the argon-adsorption data.

are indicative of micropores with average aperture diameters between 1.1–2.0 nm for MFU-4*l*. These values are in good agreement with the average pore diameters calculated from crystallographic data (1.2 nm for the pores in the **A** cell and 1.86 nm for pores in the **B** cell).[27]

However, both the results of the pore geometries derived from NLDFT calculations and the Dubinin–Radushkevich (DR) equation have to be regarded with caution and should not be over-interpreted, since the available slit-pore model in the case of NLDFT is slightly erroneous due to wrong pore geometry assumptions, and DR suffers from the fact that is does not give a realistic description of micropore filling because it is derived from classical, macroscopic theories.[23]

Hydrogen adsorption: Excess hydrogen-adsorption isotherms of MFU-4*l* up to 20 bar for temperatures between 77 K and room temperature are shown in Figure 12. At 77 K, a typical type-I isotherm is observed but saturation is not reached up to 20 bar. At 20 bar the excess hydrogen uptake is 4 wt % for 77 K and decreases with rising temperature. At room temperature the hydrogen uptake increases linearly with the pressure up to 0.1 wt %. The temperature and pressure dependence of the hydrogen uptake for MFU-4*l* is very similar to MOF-5, which shows an uptake of 4.5 wt % at 77 K and also no saturation up to 20 bar.[6] The investigated MOF-5 reference sample had a specific surface area of $2360 \text{ m}^2\text{g}^{-1}$ (nitrogen BET), which is comparable to the surface area of MFU-4*l* of $2750 \text{ m}^2\text{g}^{-1}$ (argon BET).

In Figure 13a the excess hydrogen uptake of MFU-4*l* and MFU-4 (all isotherms measured for MFU-4 are given in the
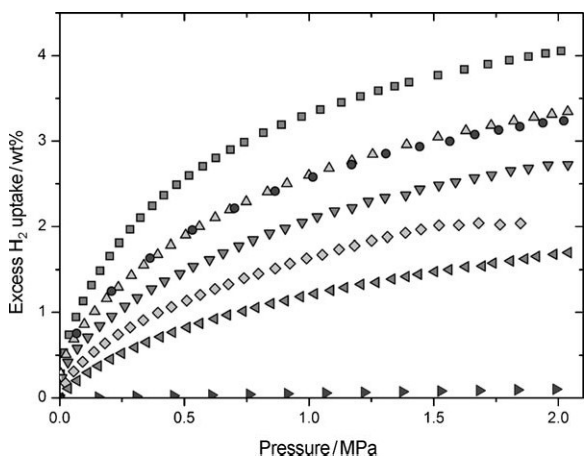
Figure 12. Excess hydrogen adsorption isotherms for MFU-4*l* at 77 K (liquid nitrogen, ■), 87 K (liquid argon, ▲), 87 K (cooling system (CS), ●), 97 K (CS, ▼), 107 K (CS, ◆), 117 K (CS, ◀), and 298 K (▶).
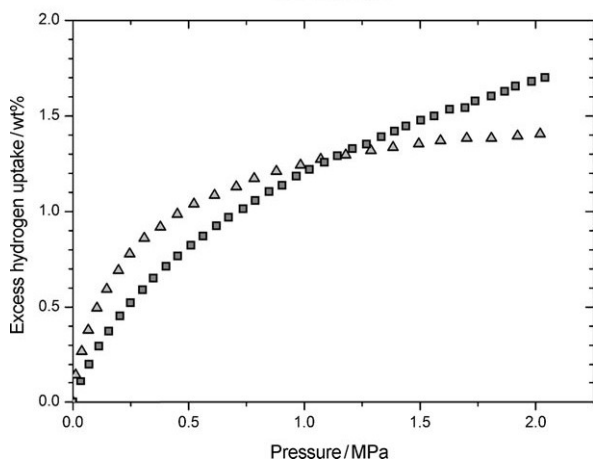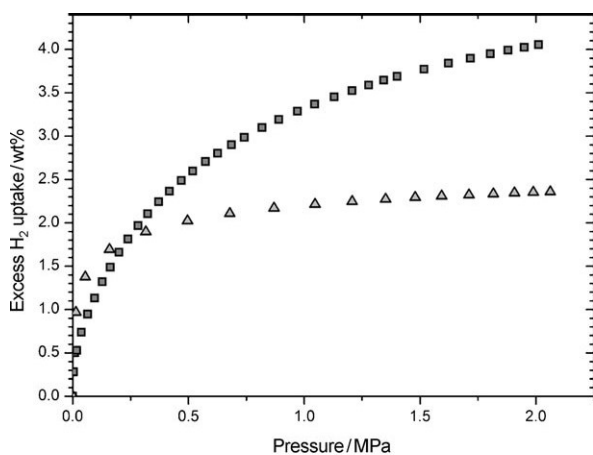

Figure 13. Excess hydrogen uptake at a) 77 K and b) 117 K for MFU-4 (triangles) and MFU-4*l* (squares).

Supporting Information) at 77 K are shown. The two isotherms cross each other at 0.24 MPa. MFU-4 stores more hydrogen at pressures below 0.24 MPa, while at higher pressures MFU-4*l* does not reach saturation and stores up to twice as much hydrogen as MFU-4 (4 wt% at 20 bar). The temperature dependence of the maximum hydrogen uptake

is different for MFU-4 and MFU-4*l*. This leads to a shift of the crossover to higher pressures at higher temperatures. For example, at 117 K the crossover is shifted from 0.24 to 1.2 MPa (Figure 13b). At 117 K and 20 bar, MFU-4 stores 1.3 wt% and MFU-4*l* just slightly more with 1.8 wt%.

The difference in the shape of the isotherm is reflected in the heat of adsorption (Figure 14). The isosteric heat of adsorption is calculated from a variant of the Clausius–Cla-
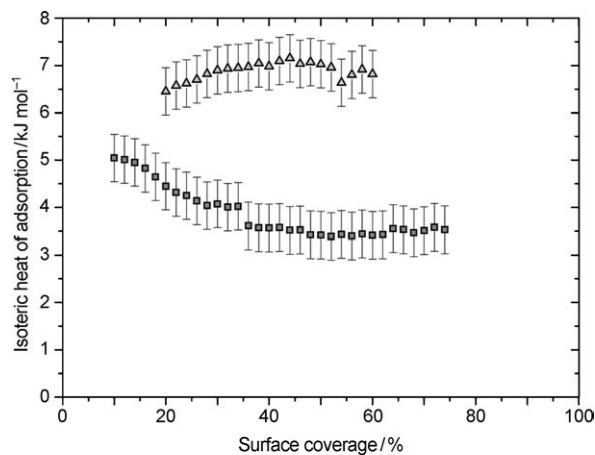

Figure 14. Isosteric heat of adsorption for hydrogen in MFU-4 (triangles) and MFU-4*l* (squares) normalized to the hydrogen uptake at 20 bar and 77 K.

peyron equation from high pressures (0–2 MPa) isotherms for intermediate surface coverage. For MFU-4 the isosteric heat of adsorption is constant within the experimental uncertainty at 7 kJ mol^{-1}, which is one of the highest heat of adsorption ever observed over such a wide range of surface coverage for hydrogen physisorption in porous materials.[6] For MFU-4*l*, the isosteric heat of adsorption at low surface coverage is approximately 5 kJ mol^{-1} and strongly decreases with hydrogen uptake. Above 30% surface coverage the heat of adsorption remains constant at 3.5 kJ mol^{-1}. This difference in the isosteric heat of adsorption is caused by the pore structure, as smaller pores lead to higher overlap of the van der Waals potentials of the wall and therefore higher heat of adsorption.[6]

Thermal desorption spectroscopy: Figure 15 shows thermal desorption spectra of hydrogen for MFU-4 and MFU-4*l* for two different heating rates, 0.1 and 0.01 Ks^{-1} in a temperature range between 20 and 120 K. At higher temperatures no hydrogen was desorbed. The TDS spectra show distinct differences in the temperature profile and in the magnitude of the signal between MFU-4 and MFU-4*l*. Furthermore, the desorption spectra measured with a slower heating rate are slightly shifted toward lower temperatures, which indicates that the hydrogen release is thermally activated. For MFU-4*l*, the majority of the adsorbed hydrogen molecules were desorbed below 60 K, whereas for MFU-4 the major hydrogen desorption just began at this temperature. The
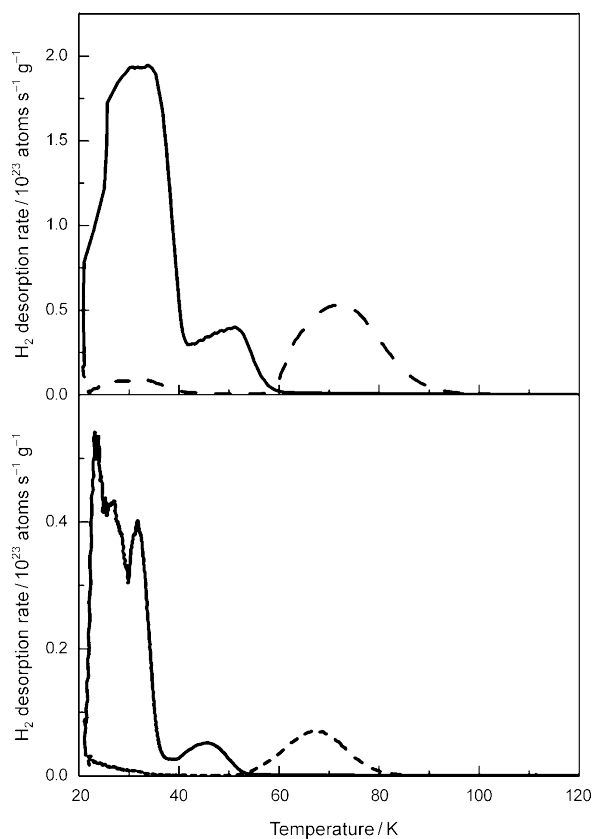
Figure 15. Hydrogen thermal desorption spectra of MFU-4 (- - - - -) and MFU-4*l* (———) recorded with a heating rate of 0.1 Ks^{-1} (top) and 0.01 Ks^{-1} (bottom).

total amount of desorbed gas, corresponding to the area under the desorption curve, was about 2.5 and 1 wt% for MFU-4*l* and MFU-4, respectively.

MFU-4*l* exhibits two hydrogen-desorption maxima, one broad and large maximum centered at approximately 32 K and a smaller maximum centered at 51 K (for a heating rate of 0.1 Ks^{-1}). During cooling under a hydrogen atmosphere a certain amount of gas is liquefied or adsorbed in multilayers giving rise to additional desorption in this low-temperature region.[7,28] For MFU-4*l* this effect gives rise to the low-temperature shoulder and the first large desorption peak for a heating rate of 0.1 and 0.01 Ks^{-1}, respectively. Nevertheless, the presence of two distinct desorption maxima for MFU-4*l* indicates clearly the presence of two hydrogen adsorption sites possessing different heats of adsorption. The larger first desorption peak at about 32 K can be assigned to hydrogen adsorbed in the cavities. The smaller maximum at about 51 K corresponds to stronger binding sites as already indicated by the higher heat of adsorption for low surface coverage in the pressure–capacity–temperature (PCT) measurements (Figure 14).

In contrast, for MFU-4 one dominant desorption maximum is observed at 71 K and a smaller signal around 30 K. The desorption signal in the low-temperature region may be caused by gas liquefied or adsorbed in multilayers. Most of

the hydrogen is desorbing at temperatures above 60 K, which is much higher than that of the other MOFs.[9] Indeed MFU-4 exhibits a desorption maximum with the highest temperature ever measured for physisorbed hydrogen on MOFs. The MFU-4 framework is constructed from smaller and larger cavities, arranged in an alternate fashion.[11] Owing to this structure, hydrogen molecules moving from one larger cavity to another must pass through a smaller cavity. Therefore, the diffusion of the hydrogen molecule through the aperture of the small cavities, with a diameter of approximately 2.52 Å, is the limiting factor for the degassing of hydrogen and gives rise to the high desorption temperature.

The total hydrogen uptake was calculated to about 1 wt% for MFU-4, in comparison to 2.5 wt% for MFU-4*l*. These values are lower than the maximum excess adsorption at high pressures and 77 K, which typically, for MOFs are correlated to the specific surface area and are independent of the compound.[7,29] The results obtained from TDS are sometimes lower, and especially if the heat of adsorption is low, part of the adsorbed hydrogen will be pumped away during evacuation already at 20 K. The lower value for MFU-4 may be caused by a partial filling of the cavities at 700 mbar and cooling down to 20 K, because the kinetics of the filling is limited by the diffusion through the small window of the smaller cavity.

Conclusion

We have successfully prepared and characterized a novel member of isoreticular MFU-4-type cubic frameworks, MFU-4*l*, constructed from BTDD^{2-} dianions and $\{Zn_5Cl_4\}^{6+}$ coordination units. The linker can be easily synthesized in three steps. Compared to solvothermal synthesis, the preparation of MFU-4*l* by microwave irradiation leads to a large reduction in reaction time. Thermogravimetric and VTXRPD analyses indicate that MFU-4*l* possesses very high thermal stability (500 °C under nitrogen). Large pore apertures of 9.1 Å allow adsorption and free diffusion of different molecules. In contrast, MFU-4, with small pore apertures of 2.5 Å, is highly selective for the adsorption of atoms or small molecules such as He or H$_2$ and it can therefore be applied in molecular sieving applications, some of which are hard to achieve with any other kinds of porous materials. MFU-4*l*, which has a much higher surface area, generally is able to adsorb more hydrogen than MFU-4. However, at higher temperatures and lower pressures MFU-4 adsorbs more hydrogen than MFU-4*l*. Moreover, the values of isosteric heat of adsorption, which is constant over a wide range of surface coverage and of desorption temperature, belong to the highest ever observed for hydrogen physisorption on porous materials. This makes MFU-4 more suitable for hydrogen adsorption than MFU-4*l*. These observations demonstrate the importance of pore size in designing new materials for hydrogen storage. Figure 16 shows a comparison of MFU-4 and MFU-4*l* frameworks. The diffusion path
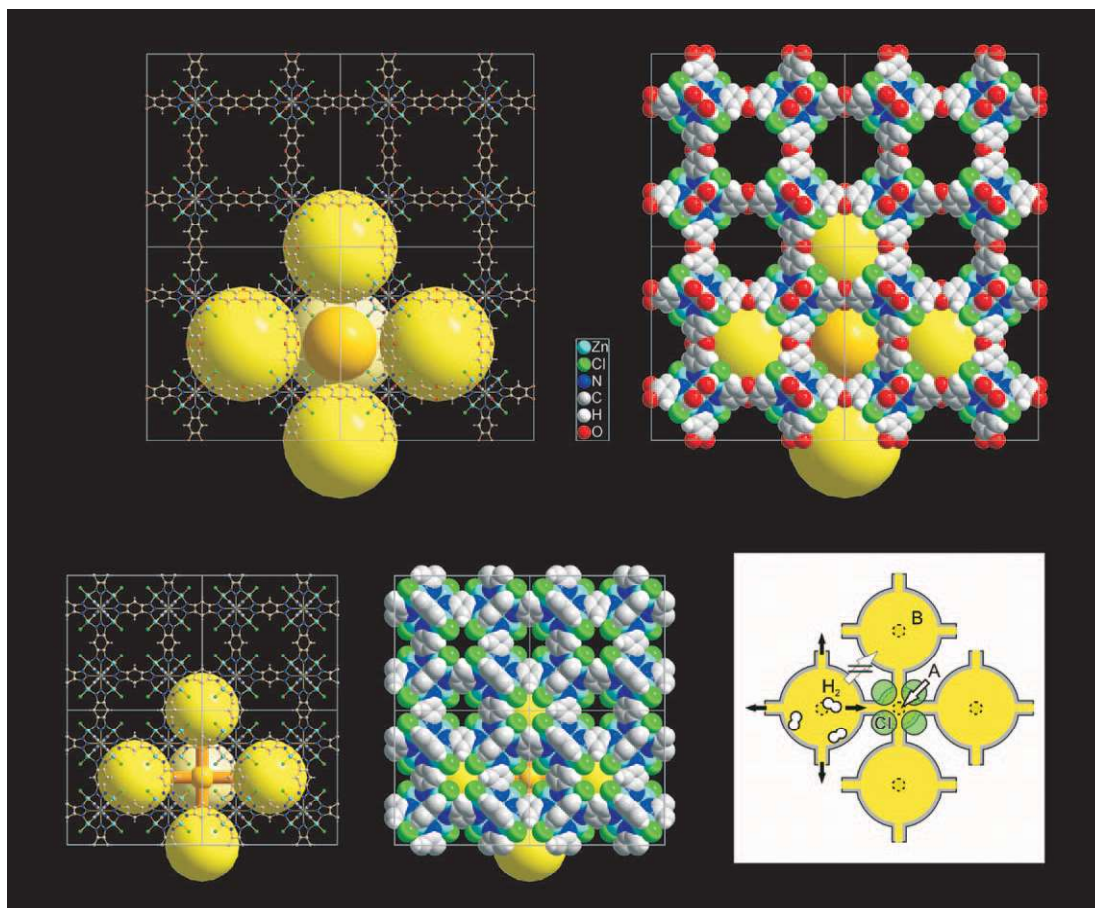
Figure 16. Frameworks of MFU-4*l* (top), MFU-4 (bottom left and middle), and the diffusion path of hydrogen molecules in MFU-4 through the aperture between **A** and **B** cells (bottom right).

of hydrogen molecules in MFU-4 through the aperture between the **A** and **B** cells is shown on the bottom right.

In conclusion, we have demonstrated that MFU-4-type frameworks have a huge potential for the development of functional materials for hydrogen storage, gas separation (MFU-4), and possible catalytic applications (MFU-4*l*). Further investigations of these frameworks are currently underway in our laboratories. For structure solution and refinement of MFU-4*l*, three-dimensional electron-diffraction data acquired by using the ADT technique was used successfully. This is the first ab initio structure solution of an unknown MOF performed with electron-diffraction data. The new ADT method delivers intensity data superior in quality and quantity and has proven to be quick, reliable, and promising for future structural investigations on MOF compounds, in which single crystals of sufficient sizes are notoriously hard to obtain.

Experimental Section

Materials and general methods: All starting materials were of reagent grade and used as received from the commercial supplier. Fourier transform infrared (FTIR) spectra were recorded from KBr pellets in the range 4000–400 cm^{-1} on a Bruker IFS FTIR spectrometer. The following indications are used to characterize absorption bands: very strong (vs), strong (s), medium (m), weak (w), shoulder (sh), and broad (br). Elemental analyses (C, H, N) were carried out on a Perkin–Elmer 2400 elemental analyzer. TGA was performed with a TGA/SDTA851 Mettler Toledo analyzer in the temperature range of 25–1100°C under flowing nitrogen at a heating rate of 10 K min^{-1}. TGA/MS analysis was carried out using Netsch thermoanalyzer STA 409 C connected to a Balzers QMG mass spectrometer by a Skimmer coupling system in the temperature range of 20–700°C under a N$_2$ flow with a heating rate of 10 K min^{-1}. Thermodesorption GC–MS analysis was carried out using Perkin–Elmer ATD 400 inlet and a Varian 3400 gas chromatograph coupled with a Finnigan Mat ITS40 mass spectrometer. The sample was heated in a glass tube at 260°C for 15 min before measurement. SEM images were recorded using a Zeiss DSM 962 scanning electron microscope. Argon-gas sorption isotherms were measured with a Quantachrome Autosorb-I ASI-CP-8 instrument. Prior to measurements, the samples of dichloromethane-exchanged MFU-4*l* were heated at 180°C for 24 h under high vacuum to remove the occluded solvent molecules. Argon-sorption experiments were performed at 77.3 K in the range of $5.00 \times 10^{-5} \leq P/P_0 \leq 1.00$ with Ar.

2,3,7,8-Tetranitrodibenzo[1,4]dioxin (3):[14] Fuming nitric acid (24 mL) was added to trifluoroacetic acid anhydride (16 mL) under cooling in an ice/water bath. Dibenzo[1,4]dioxin (5 g, 27.2 mmol) was added in small portions to a well-stirred nitration mixture while keeping the temperature below 10°C. The reaction mixture was stirred for 1.5 h at 60–70°C at reflux and then poured into ice/water (400 mL) with stirring. The precipitate was removed by filtration, washed well with water, and dried under vacuum over P$_4$O$_{10}$. Yield: 7.2 g (73%); ^{1}H NMR (400 MHz,

[D$_6$]DMSO): $\delta = 8.03$ ppm (s, 4H); ^{13}C NMR (100 MHz, [D$_6$]DMSO): $\delta = 113.8$, 138.7, 143.6 ppm; IR (KBr): $\tilde{\nu} = 3104$ (m), 3055 (m), 1641 (w), 1605 (m), 1558 (s), 1495 (s), 1431 (m), 1376 (s), 1348 (s), 1306 (s), 895 (s), 818 cm^{-1} (s); elemental analysis calcd (%) for C$_{12}$H$_4$N$_4$O$_{10}$: C 39.58, H 1.11, N 15.38; found: C 39.08, H 1.17, N 15.18.

H$_2$-BTDD·0.5 H$_2$O (2): A well-stirred mixture of compound **4** (7 g, 19.8 mmol), acetic acid (70 mL), and water (10 mL) was cooled in an ice/water bath and a solution of sodium nitrite (2.9 g, 42 mmol) in water (10 mL) was added slowly while keeping the temperature below 10°C. The mixture was diluted with water (100 mL), the precipitate was removed by filtration, washed well with water and methanol, and dried under vacuum over P$_4$O$_{10}$. Yield 3.72 g (69%); ^{1}H NMR (400 MHz, CF$_3$COOD): $\delta = 7.85$ ppm (s, 4H); ^{13}C NMR (100 MHz, CF$_3$COOD): $\delta = 99.8$, 131.1, 144.7 ppm; IR (KBr): $\tilde{\nu} = 3448$ (br), 3129 (s), 2899 (s), 2803 (s), 1711 (w), 1595 (m), 1480 (s), 1416 (m), 1355 (s), 1218 (s), 1076 (m), 1004 (m), 919 (m), 860 (s), 633 (w), 431 cm^{-1} (w); elemental analysis calcd (%) for C$_{12}$H$_7$N$_6$O$_{2.5}$: C 52.37, H 2.56, N 30.54; found: C 52.45, H 2.52, N 29.91.

[Zn$_5$Cl$_4$(BTDD)$_3$] (MFU-4*l*)

Solvothermal method: H$_2$-BTDD (760 mg, 2.77 mmol) was dissolved in DMF (760 mL) under stirring and heating at 145°C for 30 min. Anhydrous zinc chloride (7.78 g, 57.2 mmol) was added to a cooled (ca. 50°C) solution of linker and the mixture was stirred until the zinc chloride was completely dissolved. The resulting solution was heated with stirring under reflux at 145°C for 18 h and then cooled down to room temperature. The precipitate was removed by filtration, washed slowly with DMF (3×50 mL), methanol (3×50 mL), and dichloromethane (3×50 mL), and dried for 24 h at 180°C under vacuum (ca. 0.2 mbar). Yield 940 mg (90% based on ligand) of an almost white microcrystalline powder; IR (KBr): $\tilde{\nu} = 3420$ (br), 3076 (w), 2924 (w), 2854 (w), 1731 (w), 1576 (w), 1460 (s), 1346 (m), 1171 (s), 915 (m), 802 (m), 732 (w), 601 (w), 500 cm^{-1} (m); elemental analysis calcd (%) for C$_{36}$H$_{12}$Cl$_4$N$_{18}$O$_6$Zn$_5$: C 34.28, H 0.96, N 19.99; found: C 33.98, H 1.21, N 19.55.

Microwave irradiation method: H$_2$-BTDD (5 mg, 0.0188 mmol) was dissolved in DMF (5 mL) under stirring and heating at 145°C for 10 min. A 1 M solution of anhydrous zinc chloride in DMF (0.4 mL, 0.4 mmol) was added to a cooled (ca. 50°C) solution and the mixture was placed in a Pyrex sample tube (10 mL). The tube was sealed and placed in a microwave synthesizer (CEM, Discover S). The resulting mixture was heated to 155°C at 300 W, kept under these conditions for 30 min, and then cooled down to room temperature. The precipitate was removed by filtration, washed slowly with DMF (5 mL), methanol (5 mL), and dichloromethane (3×10 mL), and dried for 24 h at 180°C under vacuum (ca. 0.2 mbar). Yield 5.2 mg (73%) of an almost white microcrystalline powder. This material exhibited the same analytical results as those obtained by the solvothermal method and is phase-pure according to XRPD measurement.

Crystal structure determination by ADT: ADT[16–18] was performed in a FEI F30 TEM. The sample was deposited as a dry powder on a carbon grid and cooled to −160°C inside the microscope. An area of around 300×300 nm, on the edge of a crystal that was 1000×600 nm large, was selected for data acquisition. To have a quasi-parallel electron beam of 70 nm in diameter and a low electron dose on the sample, a C2 condenser aperture of 10 μm was inserted and a high gun lens current and spot size were used (respectively 8 and 8 for that microscope). During the tilt, the crystal position was tracked in STEM microprobe mode and the electron-diffraction patterns were collected every 1° of tilt, with an exposure time of 5 s. Two tilt series were collected with and without precession of the beam.[30] The tilt without precession, sampling a range of 60°, was used for cell-parameter determination. The tilt with precession, sampling a range of 66°, was used for intensity extraction.

All the possible 412 independent reflections up to a resolution of 1.3 Å were integrated (coverage of 100% of the reciprocal space). The internal R_{sym} was 28.63%. The isotropic thermal factor determined by a Wilson plot was 0.048 Å^2. Ab initio structure solution was performed by direct methods implemented in SIR2008[31] with a fully kinematic approach ($I = F^2$). The almost complete structure was delivered in one run. Inside the first 10 potentials, 9 corresponded to 9 atoms of the structure and 1 po-

tential to a ghost close to a Zn atom. The missing carbon atom (potential 11) was placed in a wrong special position.

The structure was refined by SHELXL.[32] The ghost disappeared during the refinement and the missing carbon atom was placed imposing a rigid benzene group. The final refinement, performed with soft restraints on bond lengths, resulted in a final residual R of 32.1%.

Crystal structure determination by PXRD: For the PXRD study, a portion of the sample was powdered and placed between two sheets of foil. Intensity data were collected using a STOE STADI P powder diffractometer with germanium monochromator, operated at 40 kV, 40 mA, Cu target; transmission geometry, fixed divergence slit 1/4°. The PXRD pattern was taken at room temperature in the 2θ range from 2.8 to 70°, step size 0.01, and time per step 596.6 s.

Variable-temperature X-ray powder diffraction (VTXRPD) measurements were performed under air or nitrogen with a PANalytical X'Pert PRO diffractometer with a X'Celerator detector operated at 45 kV, 40 mA, with Cu$_{K\alpha}$ radiation, fixed divergence slit $^1/_2$°, equipped with an Anton Paar HTK 1200N reaction chamber. Measurements were performed at a temperature range from 30 to 600°C, by employing 2θ ranges from 3.0 to 80.0°, step size 0.033° 2θ, time 98 s per step. The heating rate was 5°C min^{-1}. The sample was heated before measurement at each temperature for 15 min.

Extractions of the peak positions, pattern indexing, and determination of the lattice parameters for MFU-4*l* were carried out with the PROSZKI package.[33] Independently, the indexing process was performed by the N-TREOR09 program implemented in the EXPO2009 package.[34] Space group determination by probabilistic approach was performed by using EXPO2009. The set of the most probable space groups was found: extinction group F; space groups $F23$ (196), $Fm\bar{3}$ (202), $F432$ (209), $F\bar{4}3m$ (216), $Fm\bar{3}m$ (225). The $Fm\bar{3}m$ (225) space group was chosen for further structure determination procedures. During pattern decomposition the lattice parameters were not refined. The positions of heavy atoms Zn and Cl were found by direct methods; missing light atoms O, C, and N were localized on difference Fourier maps. Hydrogen atoms were placed in idealized position in the SHELXL program.[32]

The Rietveld refinement was carried out using the Jana2006 program.[35] Weak geometric restraints on bond lengths were used during the refinement process. No preferred orientation has been observed. Experimental details and crystal data for MFU-4*l* are listed in Table 3. The final Rietveld refinement plots are presented in Figure 17.

CCDC-776578 contains the supplementary crystallographic data for this paper. These data can be obtained free of charge from The Cambridge Crystallographic Data Centre via www.ccdc.cam.ac.uk/data_request/cif.

Hydrogen adsorption measurements: Hydrogen-adsorption measurements were performed with an automated Sieverts' apparatus

Table 3. Crystal and experimental data for MFU-4*l*.

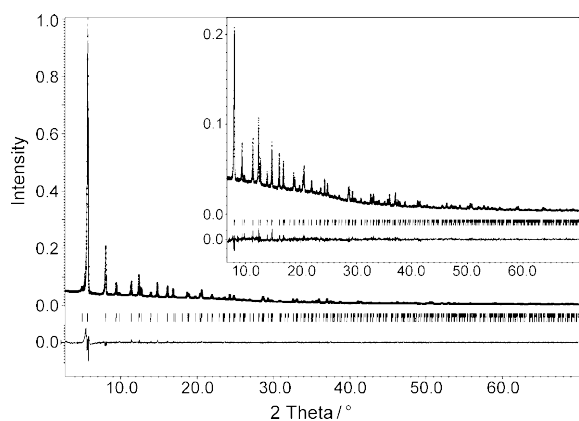| chemical formula	C$_{36}$Cl$_4$N$_{18}$H$_{12}$O$_6$Zn$_5$
formula weight	1261.32
T [K]	293(2)
2θ range [°], step size [°]	2.80–70, 0.01
X-ray source, wavelength [Å]	Cu$_{K\alpha}$, $\lambda = 1.54178$
crystal system	cubic
space group	$Fm\bar{3}m$ (225)
a [Å]	31.0569(6)
V [Å^3]	29955.2(5)
M_{30}	75.01 (0.00002, 30)
F_{30}	184.77 (0.00416, 30)
Z, ρ_{calcd} [g cm^{-3}]	8, 0.5592
no. of atoms	5
no. of observations	6720
unique reflections	315
R_p	4.63
R_{wp}	7.16
R_{obs}	5.88
R_{wobs}	5.82

Figure 17. The Rietveld refinement plots for MFU-4*l*. Dotted and solid lines represent observed and calculated patterns, respectively, with peak markers and the difference plot shown at the bottom. For clarity, the inset shows an expanded view in the range 7–70° 2θ.

(PCTPro2000, HY-Energy LLC, Setaram Inc.) and are described in detail elsewhere.[6] MFU-4*l* (115 mg) was evacuated at 180 °C overnight prior to the measurements and between each isotherm for 2 h at 50 °C. Equilibrium was reached for all pressures below 1 min. For MFU-4, two measurements were performed, first at temperatures between 77 and 117 K on a 180 mg sample and later at temperatures between 127 and 177 K on a 216 mg sample. In both experiments the sample was out-gassed overnight prior to the measurement at 250 (first sample) and 180 °C (second sample). Between individual measurements of isotherms the sample was out-gassed at temperatures above 50 °C for more than 1 h. For further analysis, results from both samples were combined.

In porous solids hydrogen is mainly adsorbed as a monolayer on inner surfaces. The amount of hydrogen that is in this adsorbed layer is called absolute adsorbed hydrogen.[36] Whereas, the excess adsorption, typically measured by taking into account the skeletal density of the material, represents the amount of hydrogen that is stored in addition to the amount of hydrogen gas that would be present in the pore volume due to external pressure. The excess adsorption is therefore smaller than the absolute adsorption by the amount of hydrogen gas that would be in the adsorbed layer if no adsorption occurred. Hence the absolute adsorption is calculated from the excess adsorption with the assumption that the adsorbed layer exhibits the density of liquid hydrogen (see the Supporting Information). The isosteric heat of adsorption is calculated from the absolute adsorbed hydrogen according to a variant of the Clausius–Clapeyron equation.[6]

Thermal desorption spectroscopy: The degassing of hydrogen was studied by low-temperature thermal desorption spectroscopy (TDS) using a special apparatus described in detail elsewhere.[28] The typical mass used is about 3 mg and the samples were out-gassed at a temperature of 440 K under high vacuum for approximately 10 h prior to the first measurement and between the measurements for at least 1 h. Then the samples were exposed to a hydrogen atmosphere (purity 99.999 %) of 700 mbar at room temperature and then cooled down to 20 K. After about 30 min at 20 K, the sample cell was evacuated. Following this, the temperature was increased with a linear heating rate (0.1 and 0.01 Ks^{-1}) from 20 to 370 K and the desorbed gases were analyzed by using a quadrupole mass spectrometer. The total number of desorbed hydrogen atoms was derived for each TDS spectrum, since the spectrometer was previously calibrated with Pd.[28]

Acknowledgements

[1] L. J. Murray, M. Dincă, J. R. Long, *Chem. Soc. Rev.* **2009**, *38*, 1294–1314.

[2] H. Frost, T. Düren, R. Q. Snurr, *J. Phys. Chem. B* **2006**, *110*, 9565–9570.

[3] S. S. Kaye, A. Dailly, O. M. Yaghi, J. R. Long, *J. Am. Chem. Soc.* **2007**, *129*, 14176–14177.

[4] S. K. Bhatia, A. L. Myers, *Langmuir* **2006**, *22*, 1688–1700.

[5] M. Dinca, J. R. Long, *Angew. Chem.* **2008**, *120*, 6870–6884; *Angew. Chem. Int. Ed.* **2008**, *47*, 6766–6779.

[6] B. Schmitz, U. Müller, N. Trukhan, M. Schubert, G. Férey, M. Hirscher, *ChemPhysChem* **2008**, *9*, 2181–2184.

[7] B. Panella, K. Hönes, U. Müller, N. Trukhan, M. Schubert, H. Pütter, M. Hirscher, *Angew. Chem.* **2008**, *120*, 2169–2173; *Angew. Chem. Int. Ed.* **2008**, *47*, 2138–2142.

[8] M. Rzepka, P. Lamp, M. A. de La Casa-Lillo, *J. Phys. Chem. B* **1998**, *102*, 10894–10898.

[9] a) M. Eddaoudi, D. B. Moler, H. Li, B. Chen, T. M. Reineke, M. O'Keeffe, O. M. Yaghi, *Acc. Chem. Res.* **2001**, *34*, 319–330; b) M. Eddaoudi, J. Kim, N. Rosi, D. Vodak, J. Wachter, M. O'Keeffe, O. M. Yaghi, *Science* **2002**, *295*, 469–472; c) H. Li, M. Eddaoudi, M. O'Keeffe, O. M. Yaghi, *Nature* **1999**, *402*, 276–279.

[10] M. Tonigold, Y. Lu, B. Bredenkötter, B. Rieger, S. Bahnmüller, J. Hitzbleck, G. Langstein, D. Volkmer, *Angew. Chem.* **2009**, *121*, 7682–7687; *Angew. Chem. Int. Ed.* **2009**, *48*, 7546–7550.

[11] S. Biswas, M. Grzywa, H. P. Nayek, S. Dehnen, I. Senkovska, S. Kaskel, D. Volkmer, *Dalton Trans.* **2009**, 6487–6495.

[12] S. Biswas, M. Tonigold, D. Volkmer, *Z. Anorg. Allg. Chem.* **2008**, *634*, 2532–2538.

[13] K. Kuratowski, *Fund. Math.* **1930**, *15*, 271–283.

[14] H. Gilman, J. J. Dietrich, *J. Am. Chem. Soc.* **1958**, *80*, 366–368.

[15] K. Chichak, U. Jacquemard, N. R. Branda, *Eur. J. Inorg. Chem.* **2002**, 357–368.

[16] U. Kolb, T. Gorelik, C. Kübel, M. T. Otten, D. Hubert, *Ultramicroscopy* **2007**, *107*, 507–513.

[17] U. Kolb, T. Gorelik, M. T. Otten, *Ultramicroscopy* **2008**, *108*, 763–772.

[18] E. Mugnaioli, T. Gorelik, U. Kolb, *Ultramicroscopy* **2009**, *109*, 758–765.

[19] U. Kolb, T. E. Gorelik, E. Mugnaioli, A. Stewart, *Polymer Reviews* **2010**, *50*, 385–409.

[20] I. Rozhdestvenskaya, E. Mugnaioli, M. Czank, W. Depmeier, U. Kolb, A. Reinholdt, T. Weirich, *Mineral. Mag.* **2010**, *74*, 159–177.

[21] a) O. I. Lebedev, F. Millange, C. Serre, G. Van Tendeloo, G. Férey, *Chem. Mater.* **2005**, *17*, 6525–6527; b) D. Chandra, M. W. Kasture, A. Bhaumik, *Microporous Mesoporous Mater.* **2008**, *116*, 204–209; c) D. Jiang, T. Mallat, F. Krumeich, A. Baiker, *J. Catal.* **2008**, *257*, 390–395; d) S. Turner, O. I. Lebedev, F. Schröder, D. Esken, R. A. Fischer, G. Van Tendeloo, *Chem. Mater.* **2008**, *20*, 5622–5627; e) F. Schröder, D. Esken, M. Cokoja, M. W. E. van den Berg, O. I. Lebedev, G. Van Tendeloo, B. Walaszek, G. Buntkowsky, H.-H. Limbach, B. Chaudret, R. A. Fischer, *J. Am. Chem. Soc.* **2008**, *130*, 6119–6130; f) S. J. Yang, J. Y. Choi, H. K. Chae, J. H. Cho, K. S. Nahm, C. R. Park, *Chem. Mater.* **2009**, *21*, 1893–1897.

[22] A. L. Spek, *J. Appl. Crystallogr.* **2003**, *36*, 7–13.

[23] F. Rouquerol, J. Rouquerol, K. Sing, *Adsorption by Powders & Porous Solids*, Academic Press, San Diego, **1999**.

[24] a) T. Düren, F. Millange, G. Férey, K. S. Walton, R. Q. Snurr, *J. Phys. Chem. C* **2007**, *111*, 15350–15356; b) K. S. Walton, R. Q. Snurr, *J. Am. Chem. Soc.* **2007**, *129*, 8552–8556.

[25] P. I. Ravikovitch, A. V. Neimark, *Colloids Surf. A* **2001**, *187–188*, 11–21.

[26] J. Jagiello, M. Thommes, *Carbon* **2004**, *42*, 1227–1232.

[27] The van der Waals radii of C (0.17 nm) and Cl (0.175 nm) were used to calculate the width of the apertures: A. Bondi, *J. Phys. Chem.* **1964**, *68*, 441–451.

[28] B. Panella, M. Hirscher, B. Ludescher, *Microporous Mesoporous Mater.* **2007**, *103*, 230−234.

[29] B. Panella, M. Hirscher, H. Puetter, U. Mueller, *Adv. Funct. Mater.* **2006**, *16*, 520−524.

[30] R. Vincent, P. A. Midgley, *Ultramicroscopy* **1994**, *53*, 271−282.

[31] M. C. Burla, R. Caliandro, M. Camalli, B. Carrozzini, G. L. Cascarano, L. De Caro, C. Giacovazzo, G. Polidori, S. Diligi, R. Spagna, *J. Appl. Crystallogr.* **2007**, *40*, 609−613.

[32] G. Sheldrick, *Acta Crystallogr. Sect. A* **2008**, *64*, 112−122.

[33] W. Lasocha, K. Lewinski, *J. Appl. Crystallogr.* **1994**, *27*, 437−438.

[34] A. Altomare, M. Camalli, C. Cuocci, C. Giacovazzo, A. Moliterni, R. Rizzi, *J. Appl. Crystallogr.* **2009**, *42*, 1197−1202.

[35] V. Petricek, M. Dusek, L. Palatinus, Jana2006. The crystallographic computing system. Institute of Physics, Praha, Czech Republic, **2006**.

[36] F. O. Mertens, *Surf. Sci.* **2009**, *603*, 1979−1984.